Progress In Electromagnetics Research B, Vol. 70, 73–85, 2016

Cogging Torque and Torque Ripple in a Direct-Drive Interior Permanent Magnet Generator

Rukmi Dutta*, Kazi Ahsanullah, and Faz Rahman

Abstract—This paper investigates the cogging torque and torque ripple in high pole number interior permanent magnet generators, designed for direct-drive applications. Two interior permanent magnet rotor topologies — flat-shaped and V-shaped were considered with distributed wound and fractional slot concentrated wound stators. A comparison of torque performances was made between distributed wound and fractional-slot concentrated wound generators. Cogging torque was minimized by finding an optimum magnet pole arc length and torque ripples were minimized by finding optimum slot-opening and flux barrier shape. Design analysis was carried out in finite element models. It was found that flat-shaped rotor topology in the fractional slot concentrated wound stator can provide the best torque performance regarding low cogging torque and torque ripple. This finding was verified in constructed prototype machine.

1. INTRODUCTION

Interior Permanent Magnet Generator (IPMG) is an emerging technology in the field of wind energy conversion. High torque density, reduced use of expensive rare earth magnet materials, high efficiency, and flux-weakening capability are making these machines competitive in the direct-drive (D-D) wind energy conversion systems. A D-D IPMG can be advantageous regarding profit and pay-back time in low average wind-speed sites because of constant power operation under flux-weakening [1]. A fractional-slot, concentrated- wound (FSCW) IPMG offers high slot fill factor, high tolerance to phase fault, simplified manufacturing process, short end-turns, reduced copper usages [2–4]. These advantages make such machines uniquely suitable for D-D wind energy conversion. In a D-D wind energy conversion system, the electromagnetic torque quality of the generator plays an important role in the system performance. The cogging torque and torque ripple of the generator can cause fatigue and stress in the mechanical structure of the turbine [5]. A compact machine, designed with strong permanent magnets and small air gap, tends to have high cogging torque [6]. D-D PM generators fall into this category. It was recommended in [7] that ideally, cogging torque of a D-D PM generator should not exceed 2% of the rated torque.

FSCW stator has been used effectively to minimize cogging torque in PM machines [2, 8, 9]. However, design tradeoff may require between cogging torque and torque ripple as found in [10] for a surface-type PM machine. In the literature, only a few papers have investigated D-D FSCW IPMG [5, 11, 12]. A preliminary analytical design of a 10 MW, 12-phase FSCW IPMSG was validated in a finite element (FE) model in [5]. A three-phase, FSCW IPMG was proposed for a 7 MW offshore wind turbine to enhance fault tolerance in [12]. The performance of the proposed machine of [12] under partial demagnetization was studied through FE simulation. Influence of winding layers on the rotor loss and torque ripple of a 3 kW FSCW IPMG was investigated in [11] using FE simulation; no experimental

Received 20 July 2016, Accepted 9 October 2016, Scheduled 20 October 2016

* Corresponding author: Rukmi Dutta (rukmi.dutta@unsw.edu.au).

The authors are with the School of Electrical Engineering and Telecom, The University of New South Wales, NSW 2052, Sydney, Australia.

verification was available. The effect of cogging torque and ripple on the magnetic force and vibration of low-speed FSCW machine was investigated in [13] using a surface-type PM rotor. None of these papers have investigated tradeoff relation between cogging torque and torque ripple in the FSCW IPMG.

This paper presents cogging torque and torque ripple analysis of a D-D FSCW IPMG which was designed to achieve goals — (i) cogging torque $< 1\%$ of rated torque and (ii) machine generated torque ripples $< 5\%$. The design process was started by comparing the performances of an FSCW stator with a conventional DW stator, having same specifications. Optimization was carried out in an FE model, and torque performances were experimentally validated in a prototype machine constructed based on the optimized design. After the introduction in Section 1, the Section 2 discusses the related theory of cogging torque and torque ripple. The design consideration to minimize cogging torque and torque ripple in the D-D IPMG are presented in Section 3. The torque performances of DW and FSCW designs are compared in Section 4 and before the concluding remarks in Section 4, the experimental verifications of a prototype machine are presented in Section 5.

2. COGGING TORQUE AND TORQUE RIPPLE

2.1. Cogging Torque

Cogging torque is the circumferential component of the magnetic force that attempts to align of the stator teeth with the pole magnet of the rotor. The peak cogging torque occurs when the interpolar axis is about to align with the edge of the stator because of the variation of magnetic energy W_m with rotor position θ is the highest at this position [14–16]. A general expression of cogging torque was given in [15],

$$T_{cog} = \sum_{i=1,2,3,\ldots}^{\infty} K_{sk} T_{i\_pk} \sin(iN_c\theta) \tag{1}$$

where, K_{sk} is the skew factor and equal to one when there is no skewing, N_c the least common multiple (LCM) of slot number Q_s and pole number P, T_{i_pk} the magnitude of the ith harmonic component of the cogging torque and θ the rotor position in mechanical degree. The number of time periods of a cogging torque during one slot-pitch rotation was derived in [16] and is given as,

$$N_p = \frac{P}{HCF\{Q, P\}} \tag{2}$$

where HCF is the highest common factor of Q and P. The cogging torque of Eq. (3) can be easily expressed in terms of N_p using the relation between LCM and HCF of Q and P. It becomes

$$T_{cog} = \sum_{i=1,2,3,\ldots}^{\infty} K_{sk} T_{i\_pk} \sin(iN_pQ\theta) \tag{3}$$

A low N_p means peaks of all the elementary torques due to the interaction of slot opening and the edge of the magnet pole occurs at the same rotor position and adds up to result in a significant peak cogging torque. Contrary to this, a high N_p means the peaks of elementary torques are distributed along the slot pitch resulting in lower peak cogging torque but with higher fundamental frequency. The period of a cogging torque can be expressed as,

$$\tau_p = \frac{360^\circ}{LCM\{Q, P\}} \tag{4}$$

Thus, a high LCM value or low HCF value of Q and P minimizes cogging torque. Since the position of the pole magnet edge with respect to the slot opening is closely related to the peak cogging torque, the geometrical parameters such as length of the pole magnet arc and slot openings are crucial in minimizing cogging torque. The skewing of pole magnet and stator teeth can also minimize cogging torque by creating an offset between the slot opening and the pole magnet edge.

2.2. Torque Ripple

The spatial harmonics of the stator magnetomotive force (MMF) that rotates asynchronously with the rotor cause variation of flux across the flux barriers of the rotor [17]. At the same time, there are high order harmonics in the airgap flux density of the rotor due to its the rectangular distribution [18]. Interaction of these unwanted harmonics produces torque ripple in an IPM machine. An analytical expression of torque ripple regarding rotor and stator MMFs was derived for a DW IPM machine in [19] and is given as follows,

$$T_{ripple} = -\frac{P}{2}\frac{\mu_0}{g} r_g l \pi \sum_{\substack{n = 6m \mp 1 \\ m = 1, 2, 3, \ldots}} (n f_{s,n} f_{r,n} \sin((n \pm 1)\theta_r \pm \gamma_d)) \tag{5}$$

where, P = number of poles; r_g = airgap radius; l = stack-length; g = airgap length; n = harmonic number; θ_r = rotor angular position (electrical); γ_d = current angle measured from d-axis; $f_{s,n} = n$th-order stator MMF harmonic; $f_{r,n} = n$th-order rotor MMF harmonic.

The above expression is valid of an FSCW IPM machine with the exception that the main torque producing harmonic in such a machine is not the fundamental but its order is equal to pole-pair number. A winding function specific to an FSCW stator should be used to derive stator MMF f_s in Eq. (5). However, the two key observation made in [19] about the amplification of torque ripple by the harmonic order $n = 6m \mp 1$ and null contribution from the even order harmonics are valid in an FSCW IPM machine. Thus, by reducing the discontinuity effect of the stator slots and rotor flux barriers in the MMF waves, the higher order harmonics and hence, the amplitude of the torque ripple can be minimized.

3. IPMG DESIGN CONSIDERATION

In this paper, the IPMG was designed to achieve the specifications given in Table 1. Two types of stator — conventional distributed wound (DW) and FSCW, and two kinds of magnet configurations — flat-shaped and V-shaped, both with one magnet layer per pole were investigated. The IPMG with flat-shaped and V-shaped magnet configurations are referred as IPMG-F and IPMG-V. Fig. 1 shows the cross-sectional views of rotor magnet poles IPMG-F and IPMG-V. Minimization of cogging torque and torque ripple were attempted without skewing the rotor magnet or stator tooth to avoid manufacturing complexity.

Table 1. Design specification of the D-D IPMG.

Power	4 kW
Current	6.5 A
Voltage (L-L)	362 V (rms)
Torque	267 Nm
Speed	143 rpm
Pole numbers	42
Rated frequency	50 Hz
Magnet remanence	1.16 T (NdFeB)
Phases	3

3.1. Winding Structure

For a D-D generator, sometimes, a full-pitch over a short-pitch DW stator was preferred to achieve a compact size. However, in this paper, a short-pitch winding of 6 slots per pole was selected, which had higher N_c than a 3-slot-per-pole, full-pitch winding. In the case of an FSCW stator, selection of the slot

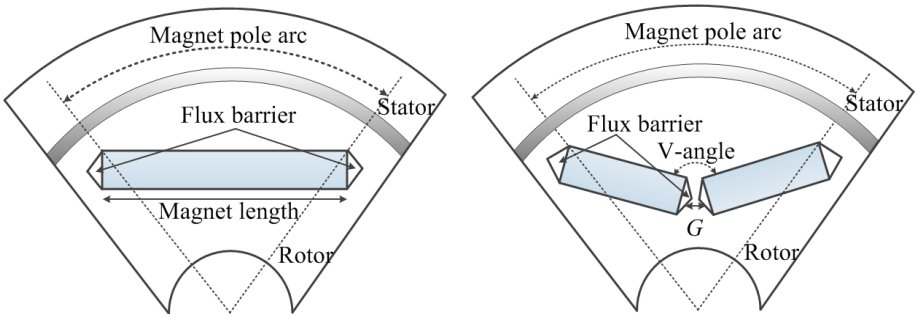

Figure 1. Cross-sectional view of one rotor pole, (a) flat-shaped (IPMG-F) and (b) V-shaped (IPMG-V).

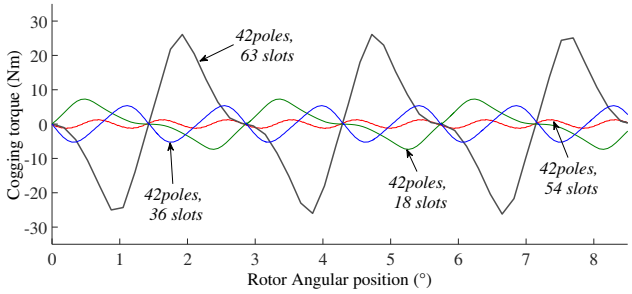

Figure 2. Cogging torque of the 42 pole IPMM with various slot combinations.

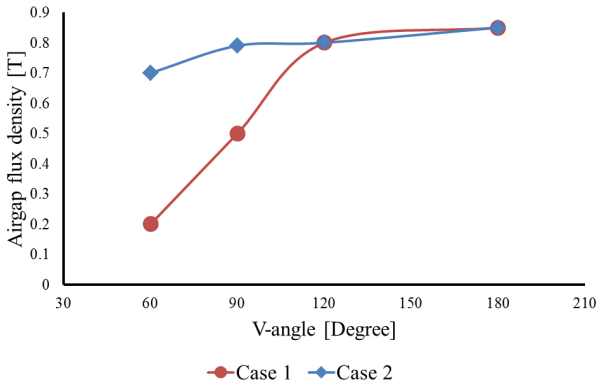

Figure 3. Variation of fundamental component of airgap flux density for case 1 (constant magnet pole arc) and case 2 (constant magnet surface area).

numbers is not as straightforward as a DW stator. In an FSCW machine, only certain combinations of slots and poles result in a fundamental winding factor greater than 0.9. Selection of slot number becomes further restricted to the multiples of two times of phase number (i.e., 6 for a 3-phase machine) if a double-layer winding is considered. Double-layer FSCW machines produce sinusoidal EMF, and low magnitude of sub-harmonics in the MMF waveform, which are beneficial to obtain low rotor iron losses and to reduce torque ripple caused by unbalanced saturation of poles [20]. It can be shown using the synthesis given in [4, 21] that for a 42-pole machine considered in this study, two of the possible slot numbers in a double layer structure that provide winding factor > 0.9 are 36 and 54. Fig. 2 shows the cogging torque waveform for all possible fractional slot winding structure of a 42 pole IPMM. It is evident from the Fig. 2 that the cogging torque is lowest for a 42 pole 54 slot machine as the LCM is highest in comparison to the other configurations. Additionally, if the slot number is less than the pole number, the machine becomes subjected to magnetic unbalance. Therefore, slot number 54 is selected for this study. The 42-pole and 54-slot structure gives slot per pole per phase, S_{pp} equal to 3/7.

3.2. Rotor Magnet Topologies

In this study, two magnet configurations shown in Fig. 1 are considered. One of the challenges in the design of D-D, low-speed machine is the optimum placement of a larger number of poles in an optimally sized rotor to obtain a most compact design. From the geometry of pole pitch in an IPMG-F, it can be shown that the length of a pole magnet is limited by the rotor radius and pole numbers, which can be

expressed as Eq. (6).

$$t_m < 2R_r \times \cos\left(\frac{\pi}{P}\right) \tag{6}$$

where, t_m is magnet length, R_r is rotor radius.

The limit of magnet length can be relaxed to a certain extent in a V-shaped configuration by reducing the angle between the two magnet pieces of one pole. This angle is referred as V-angle in Fig. 1(b). A flat-shaped configuration can be considered as having a V-angle of 180°. However, in V-shaped configuration, the V-angle influences performances of the machine greatly [22]. Therefore, finding an optimum value of V-angle is paramount in the design of an IPMG-V. Open circuit airgap flux density is a key performance indicator of a PM machine. Airgap flux density of an IPM rotor with various V-angles with a DW stator was calculated in a 2D FE model of a DW IPMG-V. The key dimensions given in Table 2 are kept constant in all models. It should be noted that variation of the V-angle may result in unacceptably large flux leakage in some designs if proper care is not taken. The large leakage is caused by the widening of the iron bridge between the two magnets legs (referred "G" in Fig. 1(b)) with the reduced V-angle, if the magnet pole arc length is kept fixed. To avoid such leakage, if the width of G is kept fixed while varying the V-angle, surface area of the pole magnet does not remain constant. Therefore, the comparison is carried out as two separate cases.

- Case 1: The magnet pole arc length was kept fixed, and width G was minimized by allowing magnet surface area to vary for each V-angle.
- Case 2: The magnet surface area and width G were kept fixed while the magnet pole arc length was allowed to vary with the V-angle variations.

Table 2. Key dimension of the IPMG.

Quantity	Values (mm)
Stator outer radius	340
Rotor outer radius	310
Airgap length	1.1
Stack length	162

Figure 3 compares the fundamental components of airgap flux density for various V-angle. The airgap flux density of the flat-shaped magnet referred in Fig. 3 as V-angle of 180°. The airgap flux density of the flat-shaped design was the highest due the absences of leakage path G. Air-gap flux density reduces more sharply with the V-angle for the case 1 than that of case 2. It can be concluded from this comparative study that that V-angle below 120° is not beneficial in a 42-pole machine, especially if the pole arc length needs to be fixed at an optimum value to minimize cogging torque. It should be noted that the pole pitch angle is relatively large in a low pole number machine, and decreasing of V-angle with constant magnet surface area (case 2) may result in a wide interpolar region. Consequently, a large flux concentration can occur near the center of the pole while nearly zero flux crosses to the airgap in the interpolar region. The resultant airgap flux density waveform is very peaky and may give a misleading outcome of large flux-density with narrow V-angle. Fortunately, the chance of such peaky waveform occurring in a large pole number machine with small pole pitch angle is relatively low.

3.3. Magnet Arc Length

A study was conducted on IPMG-F and IPMG-V with DW and FSCW stators to find an optimum magnet arc length for minimizing cogging torque. For this study, V-angle of the V-shaped design was kept fixed at 120°. In an IPM machine, the minimum cogging torque occurs only at one particular value of magnet arc length. If this length increases or decreases from the optimum value, cogging torque starts to grow. Cogging torque of the four designs (DW IPMG-F DW IPMG-V, and FSCW IPMG-F, FSCW IPMG-V) were computed using 2D FE analysis for various magnet arc length to find

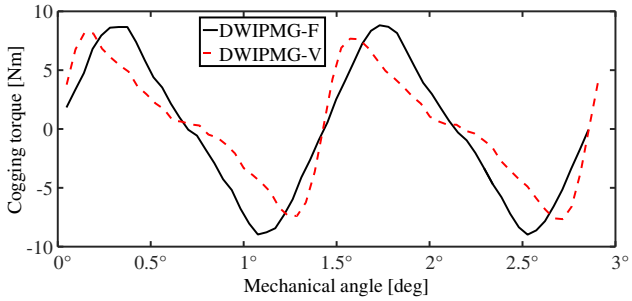

Figure 4. Cogging torque waveform of DW IPMG-F and -V.

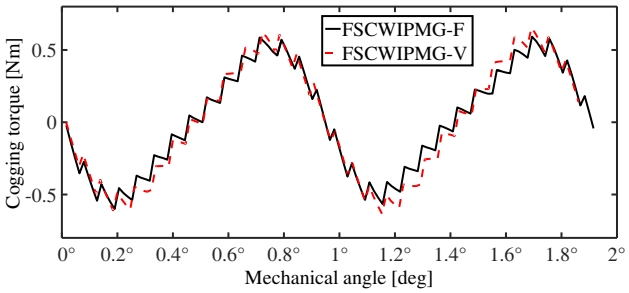

Figure 5. Cogging torque waveforms of FSCW IPMG-F and -V.

the optimum length. Fig. 4 compares the cogging torque waveforms of DW IPMG-F and -V calculated with their optimum magnet arc length. The peak of the minimum cogging torque of DW IPMG-F is slightly higher than that of the DW IPMG-V. The peak cogging torque of a DW IPMG is nearly 3% of the rated torque.

A similar optimization study of the magnet arc length was conducted for the FSCW IPMG designs. Fig. 5 compares the cogging torque waveforms of FSCW IPMG-F and -V calculated with optimum magnet arc length. The cogging torque of the FSCW IPMG designs was nearly 13 times lower than that of the DW IPMG. The V-shaped rotor has slightly higher peak cogging torque than that of the flat-shaped rotor when used with FSCW stator. The peak cogging torque of an FSCW IPMG is nearly 0.2% of the rated torque specified in Table 1.

3.4. Flux Barrier Shape and Slot Openings

Flux barriers of the rotor pole magnets and slot openings in the stator influence the ripple in the induced electromagnetic torque [23]. The torque ripple can be minimized by optimizing the shape of the flux barriers. In this study, three flux barrier designs -A, B, C as shown in Fig. 6 were considered. Induced electromagnetic torque with the rated current was calculated from the FE models with flux barrier A, B, and C for various slot opening values. The torque ripples of each case were computed as a percentage of the average induced torque. Fig. 7 compares the torque ripple of three flux barrier designs for various slot openings in DW IPMG-F and -V. Torque ripple increases with slot-opening for all three flux barrier designs in both machines. In the DW IPMG-F, flux barrier shape has minimum effect when slot opening was increased from 1.2 mm. In the DW IPMG-V, increased width of slot opening had least effect on torque ripple with flux barrier B. In both DW IPMG-F and -V, minimum torque ripple was obtained with slot opening of 1.2 mm. A slot opening smaller than 1.2 mm causes practical difficulties in winding automation and hence, such slot openings were not considered in this study. A torque ripple less than 10% of the average torque cannot be achieved in the DW IPMG-V with 1.2 mm slot opening and the three flux barrier designs considered in this study.

In the FSCW IPMG, the positioning of the slots with respect to flux barrier is not the same as the DW IPMGs. To evaluate the flux barrier designs, first, torque ripple was calculated for a fixed slot opening of 1.2 mm in the FSCW IPMG. Table 3 summarizes the effect of the three flux barrier designs on the torque and torque ripple of the FSCW IPMG-F and -V. It can be seen from the Table 3 that the flux barrier designs affect more the average torque than the torque ripple in FSCW IPMG-F. Conversely,

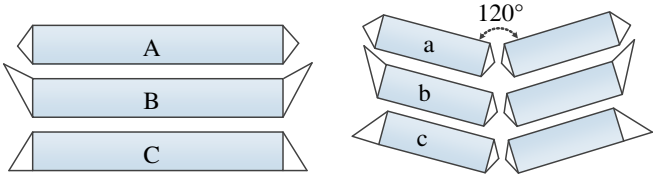

Figure 6. Three flux barrier designs for flat-shaped and V-shaped IPMGs.

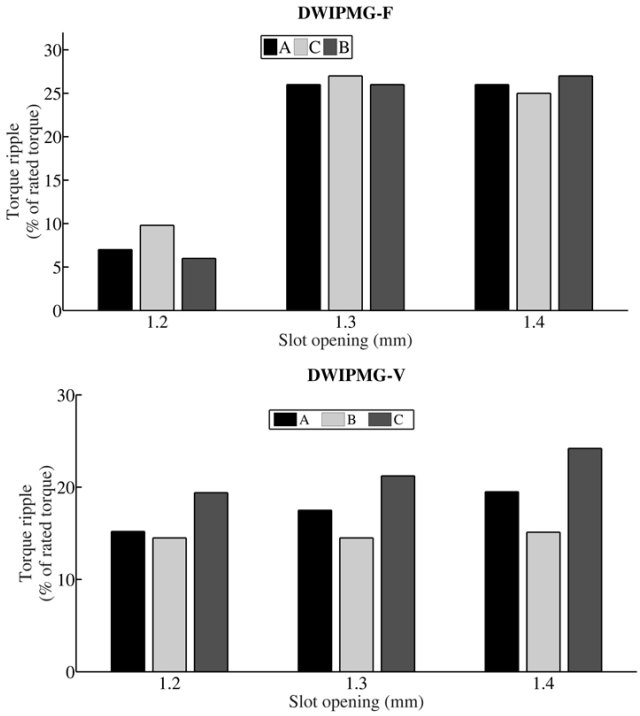

Figure 7. Torque ripple variation with slot opening width for DW IPMG.

Table 3. Average torque and torque ripple in a FSCW IPMG-F and -V.

	FSCW IPMG-F		FSCW IPMG-V	
Flux barrier design	Average torque [Nm]	Torque ripple	Average torque [Nm]	Torque ripple
A	274.8	5.8%	259.2	1.52%
B	281	5.7%	257.1	2.98%
C	272.5	4.97%	247.2	4.12%

flux barrier designs have a greater influence on the torque ripple in an FSCW IPMG-V. Considering both the average torque and torque ripple, flux barrier design 'B' gives the best performance in the FSCW IPMG-F and design 'A' produced the minimum torque ripple for the maximum average torque in the FSCW IPMG-V.

The variation of torque ripple with slot opening was investigated for both the FSCW IPMG-F and -V but with fixed flux barrier design of 'B' for FSCW IPMG-F, and 'A' for the FSCW IPMG-V. Fig. 8 shows the variation of torque ripple with the slot openings for these two machines. The widening of slot opening has a much larger effect on the FSCW IPMG-V. The ripples increase in this machine as the slot opening width increases. In FSCW IPMG-F, change in torque ripples with slot opening width is different from that of the FSCW IPMG-V. In this machine, a decreasing trend can be observed initially when slot opening is widening and after about 2 mm, torque ripples remains nearly unchanged with increased slot opening width.

4. COMPARISON OF TORQUE PERFORMANCES

A comparative study was conducted among the four designs considered for D-D generator application to evaluate the best performing design regarding average torque, torque ripple, and cogging torque. As before, key dimensions were same for all four designs, which were provided in Table 2. However,

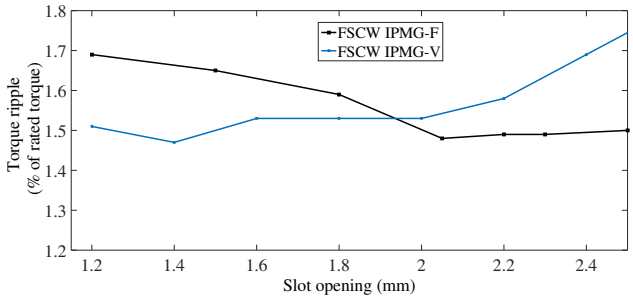

Figure 8. Variation of torque ripples with slot opening in FSCW IPMG -F and V.

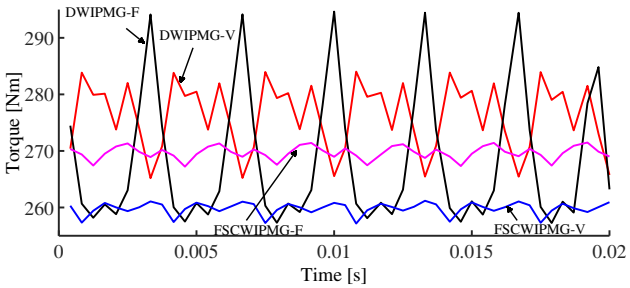

Figure 9. Developed torque of DWIPMG-F, DWIPMG-V, FSCW IPMG-F and FSCWIPMG-V.

the magnet pole arc length, the flux barrier shape, and the slot opening width of each design were selected such that minimum cogging torque, minimum torque ripple, and maximum average torque can be obtained.

4.1. Average Torque and Torque Harmonics

The developed electromagnetic torque with the rated current was calculated for each design in the FE models. Fig. 9 shows the developed torque waveforms of the four designs. The FSCW IPMG-V produces the lowest average torque, and the DWIPMG-V has the highest peak to peak torque ripples among the four designs considered in this study. Fig. 10 shows the spectrum of torque harmonics of the four machines. As expected, dominate harmonics in both DW and FSCW are 6 and its multiples. The DW IPMG-V has the largest whereas FSCW IPMG-V has the smallest 6th order harmonics among the four designs.

4.2. A Comparison Summary

Average torque, peak cogging torque and torque ripple of four designs are compared in Table 4. The optimum flux barrier design and slot opening width of each design are also shown. The total amount of rare-earth magnet used in each design is provided in the table for comparison purpose. The cogging torque and torque ripple both are much smaller in the FSCW IPMG than in the DW IPMG. However, the highest average torque was achieved in the DWIPMG-F. The DW IPMG-V has the highest torque ripple, although it requires slightly less amount of rare earth magnet. Contrary to this, FSCW IPMG-V requires more magnet material and yet produces the lowest average torque. Since the increase of slot opening width has minimum effect on the torque ripple of the FSCW IPMG-F, a larger width can be selected in this machine. Regarding torque performance and rare earth magnet volume, FSCW IPMG-F outperforms other three designs. This machine was chosen for a prototype construction and further study.

Table 4. Final results of all four designs after applying the cogging torque and torque ripple minimization techniques.

Machine designs	Flux barrier design	Slot opening width [mm]	Magnet volume [m^3]	Average Torque [Nm]	Peak cogging torque [Nm]	Torque ripple (% of average torque)
DW IPMG-F	B	1.2	0.81	276	8.81	6%
DW IPMG-V	B	1.3	0.78	265	7.67	14.4%
FSCW IPMG-F	B	2.0	0.75	270	0.655	1.48%
FSCW IPMG-V	A	1.4	0.79	260	0.61	1.47%

4.3. Design Tradeoff for Minimum Cogging Torque

An additional study was conducted on the FSCW IPMG-F to analyze the relation between minimization of cogging torque and torque ripple. For this purpose, two different magnet lengths were considered- (i) length was non-optimum for cogging torque minimization and (ii) optimum length to get minimum cogging torque. The flux barrier shape was fixed as design B for this analysis, since this shape found to produce the minimum torque ripple. The peak to peak torque ripples for various slot openings were obtained from the two FE models of the FSCW IPMG-F in which the magnet pole lengths were set as (i) and (ii). Results of this study presented in Fig. 11 shows that without optimum magnet length, the increased slot opening has a much larger effect on the overall torque ripple. It can be concluded from this study that increase in the overall torque ripple due the slot opening width is nominal when the cogging torque is minimum in an FSCW IPMG-F. However, if the non-optimum magnet length is larger than the optimum magnet length, the average torque will be larger. Thus, there is a trade-off between average torque and overall torque ripple in the machine.

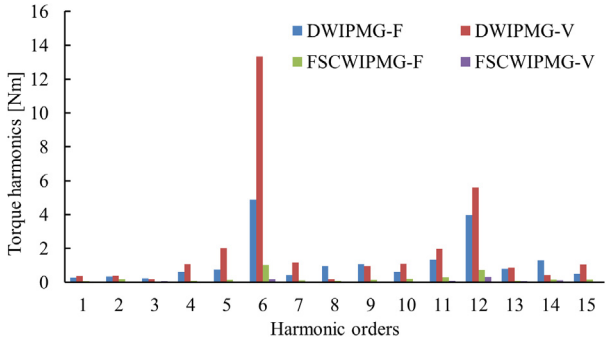

Figure 10. Torque harmonics of DWIPMG-F, DWIPMG-V, FSCW IPMG-F and FSCWIPMG-V.

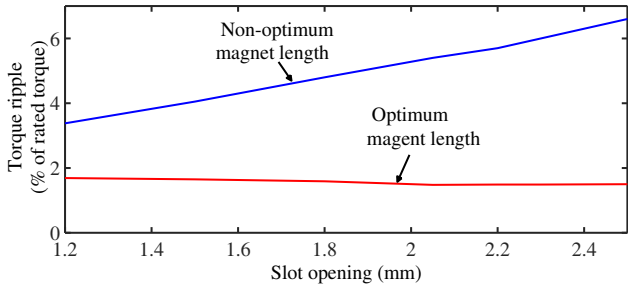

Figure 11. Variation in torque ripple with the change in slot openings for the FSCW IPMM-F with non-optimum and optimum magnet arc length of minimum cogging torque.

5. EXPERIMENTAL VALIDATION

For experimental validation, a prototype FSCWIPMG-F was constructed. Before the construction, the design was further optimized to include the dimensional tolerances. For ease of inserting magnet pieces in the cavity, a small tolerance of 0.26 mm was required during the manufacturing process. It was found through an FE analysis that such small non-magnetic cavity around the magnet pieces increases the torque ripple and the cogging torque. The torque ripple rose from 1.48% to 1.7%, and the peak cogging torque increased nearly 2 times. However, both these increase were still within the limit of the set goal. Due to the small pitch angle in large pole number machines such as direct-drive IPMG, small manufacturing tolerance in the rotor can lead to a substantial increase of cogging torque and torque ripple. Therefore, care must be taken while manufacturing such machines. Fig. 12 shows the laminations of rotor and stator, and the constructed prototype machine.

The cogging torque of the machine was measured using a static measurement method described in [24]. In this approach, the force required to move the rotor from one equilibrium state to the next stable position was measured. The absolute magnitudes of the static cogging torque were found at the selected rotor position by measuring the required force. An incremental encoder connected to the shaft was used to measure the rotor positions, and the required force was measured with standard weights. The experimental setup is shown in Fig. 13. The limitation of this method is that only increase of the cogging torque to the positive peak can be measured. However, as seen in Fig. 5, the cogging torque waveform is symmetrical in the positive and negative cycle and hence, the measurement of positive direction can be easily translated to negative side by using a non-linear curve-fitting technique such as a least-square method. Fig. 14 compares the FE predicted cogging torque to the measured cogging

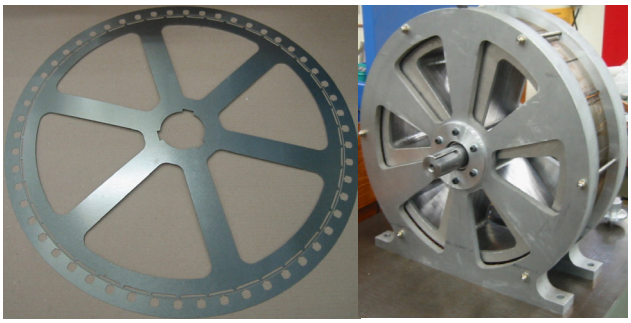

Figure 12. Lamination of rotor and stator prototype and the constructed prototype machine.

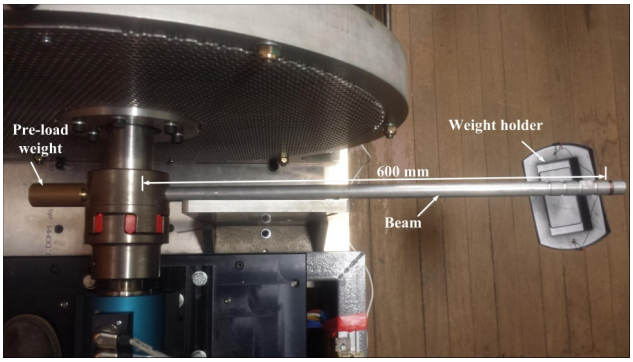

Figure 13. Experimental set-up of cogging torque measurement.

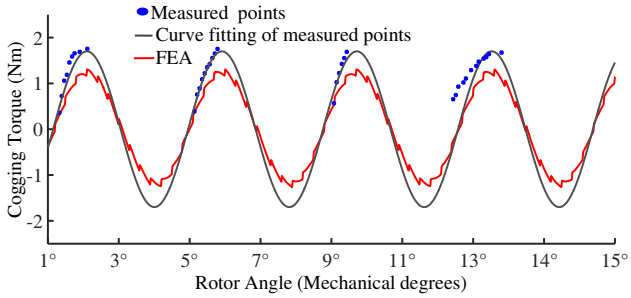

Figure 14. Experimentally measured and predicted cogging torque of the prototype FSCW IPMG-F.

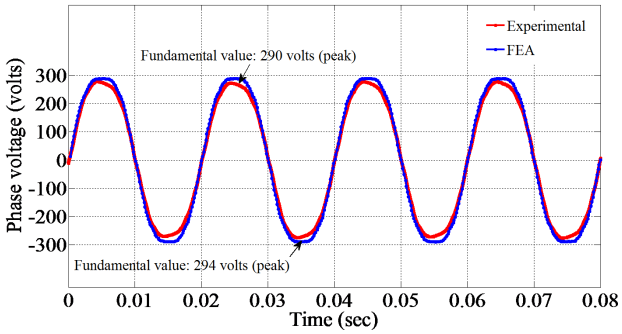

Figure 15. Open circuit back EMF (phase-neutral) at rated speed of 143 rpm.

torque. It should be noted that period of cogging torque based on Eq. (5) for the prototype machine is 0.95°. Thus, it required measuring the cogging torques at small position steps. The measured peak cogging torque was 1.76 Nm, which is about 36% larger than the FE predicted peak cogging torque. However, the measured cogging torque was still well below 1% of the rated torque. Although, care was taken to achieve the ideal geometry of the FE model in the constructed prototype, introduction of manufacturing related non-linearity could not be avoided. Some of such nonlinearities are anisotropy added to the lamination by the laser cuttings, dimensional tolerances, and presence of small amount of rotor eccentricity caused by the mounting on the bearings [25]. Manufacturing-process- introduced-nonlinearities resulted in the difference between the measured and predicted cogging torque in Fig. 14.

The machine was turned at rated speed of 143 rpm to measure the open-circuit EMF waveform. A four-quadrant dynamometer was used to drive the generator. Fig. 15 compares the measured EMF waveform (phase to neutral) to the predicted waveform of the FE model. High order harmonics in the open circuit EMF gives an indication of the contribution of the rotor MMF to the torque ripple. Fig. 16 compares the EMF harmonics of the measure, and the FE predicted waveform. The magnitudes of the FE predicted harmonics were slightly higher than the measured ones. The higher magnitudes in the FE is due to the minor differences in the remanence values of the magnet pieces in the constructed machine. According to, harmonic order 5, 7, 11, 13, ... contribute to the torque ripple. It can be seen in the Fig. 16 that these harmonics in the back EMF waveform are significantly small. Similar to the rotor, harmonics of the stator current induced MMF that contributes to the torque ripple can be observed. In this study, harmonic spectrum of the stator current induced MMF was considered in Fig. 17. It was obtained from the FE model by setting the magnet contribution to zero while stator windings were carrying the rated current. The spectrum contains sub-harmonics and the main harmonic. The main harmonic rotates synchronously with the rotor and participates in the torque production. For the

prototype FSCW IPMG-F, the main harmonic occurs as 21st harmonic, which is the pole pair number of this machine. Any odd harmonics of $6m \mp 1$ the order contributes to the torque ripple as discussed in Section 2. In the prototype machine, only such harmonic which has some significant magnitude is the 41st harmonic. All other harmonics with significant magnitude contributes to the rotor losses.

To measure the load torque characteristic, the prototype machine was loaded with a 3-phase resistive bank while driven by a four-quadrant dynamometer at rated speed of 143 rpm as shown in Fig. 18. The shaft torque of the machine was measured by a torque transducer (Kistler 4503 A with accuracy ± 0.1 Nm) and was shown in Fig. 19. The measured peak to peak torque ripple under near rated condition was found to be 13.5 Nm which was about 5% of the rated torque. Although peak to peak torque ripple of the machine was fairly small, but it was nearly two times larger than the FE predicted ripple. In the FE calculation, no external mechanical influence and any controller induced torque ripples were considered. It should be noted that the dynamometer used for driving the generator in the experimental set consists of an induction machine which has no cogging torque. Moreover, the torque measurement conducted by the torque sensor has some inertial loads added to the ripple due to minor variation in speed of the rotor [26]. However, controller induced torque ripples superimposed on the shaft torque was not filtered during these measurements.

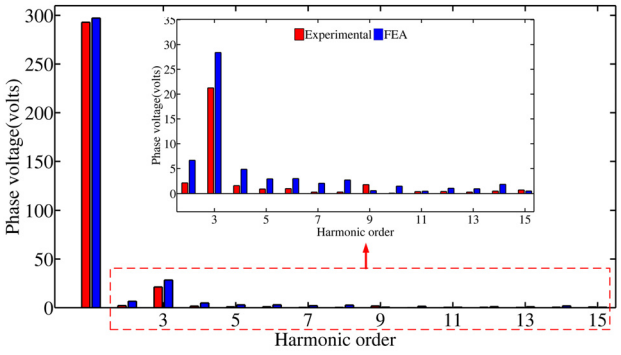

Figure 16. Harmonic spectrum of measured and FE predicted EMF waveform.

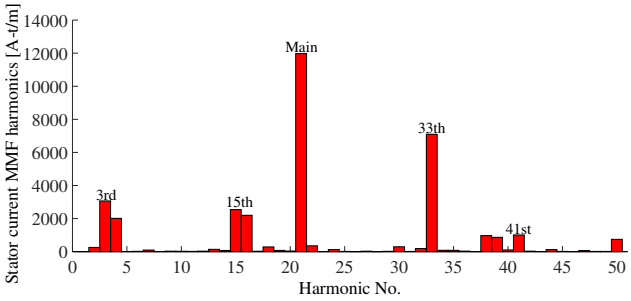

Figure 17. Stator MMF harmonics of the prototype machine obtained from the FE model.

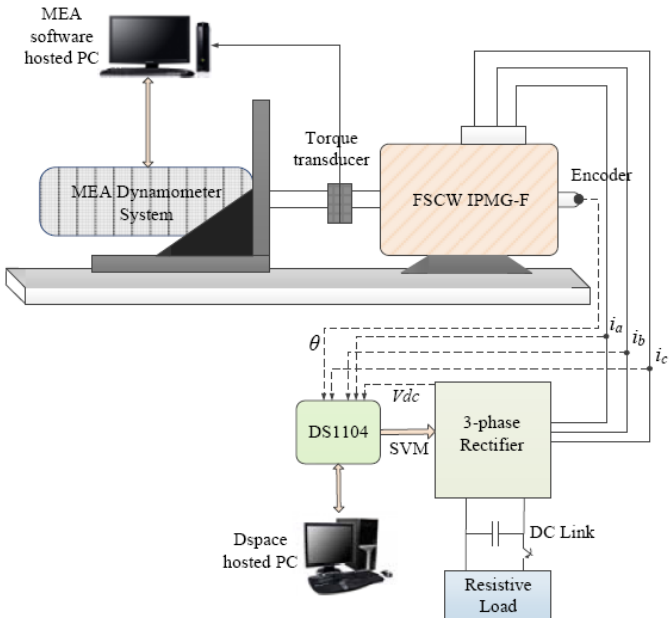

Figure 18. Experimental setup of the prototype FSCW IPMG-F.

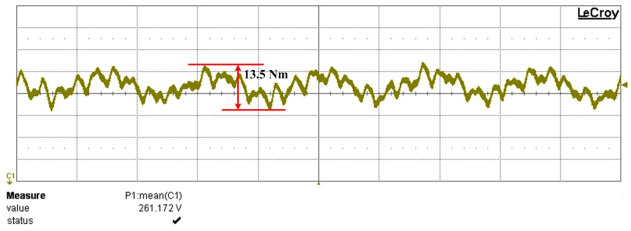

Figure 19. Experimentally measured shaft torque of the prototype FSCW IPMG-F.

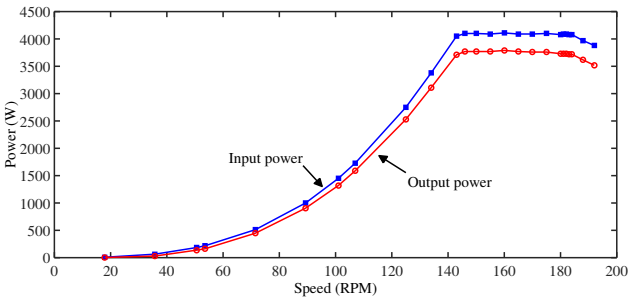

Figure 20. Experimentally measured power versus speed characteristic of the prototype FSCW IPMG-F.

The input power of the generator was calculated for various speeds using the measured shaft torque and speed and output power was measured at the load using a power analyzer during the experimental setup shown in Fig. 18. Fig. 20 shows the power versus speed characteristic of the generator. Note that, the machine goes into flux weakening once the speed increases above 143 rpm. This means that the power will remain constant as seen in Fig. 20.

6. CONCLUSIONS

An investigative study of cogging torque and torque ripple in high pole number IPMG was conducted. Two types of IPM rotor topologies — conventional flat-shape and V-shape, and two types of stator — conventional distributed wound and fractional-slot concentrated wound were considered. A comparison of the torque performance showed that flat-shaped topology is more favorable in high pole number structures. Regarding low cogging torque and torque ripple, FSCW stator performs much better than a conventional DW stator. Due to the small pitch angle, any minor change in the dimensions of pole magnet cavity to include manufacturing tolerance can increase cogging torque and torque ripple of the machine. Therefore, care should be taken during the design optimization process to include such dimensional tolerances. FSCW stator combined with flat-shaped IPM rotor topology found to be capable of minimizing cogging torque below 1%, and the torque ripple below 5% of the average torque in a direct-drive IPM generator.

ACKNOWLEDGMENT

The authors are with the School of Electrical Engineering and Telecommunications, UNSW, Australia. (email: rukmi.dutta@unsw.edu.au).

REFERENCES

1. Morandin, M., E. Fornasiero, S. Bolognani, and N. Bianchi, "Torque and power rating of a wind-power PM generator drive for maximum profit-to-cost ratio," *IEEE Transactions on Industry Applications*, Vol. 49, 866–872, 2013.
2. Dutta, R., L. Chong, and M. F. Rahman, "Design and experimental verification of an 18-Slot/14-pole fractional-slot concentrated winding interior permanent magnet machine," *IEEE Trans. Energy Convers.*, Vol. 28, 181–190, 2013.
3. El-Refaie, A. M., "Fractional-slot concentrated-windings synchronous permanent magnet machines: opportunities and challenges," *IEEE Trans. Ind. Electron.*, Vol. 57, 107–121, 2010.
4. Cros, J. and P. Viarouge, "Synthesis of high performance PM motors with concentrated windings," *IEEE Trans. Energy Convers.*, Vol. 17, 248–253, 2002.
5. Damiano, A., I. Marongiu, A. Monni, and M. Porru, "Design of a 10 MW multi-phase PM synchronous generator for direct-drive wind turbines," *Industrial Electronics Society, IECON 2013 — 39th Annual Conference of the IEEE*, 5266–5270, 2013.

6. Chang Seop, K. and S. Jin-Soo, "New cogging-torque reduction method for brushless permanent-magnet motors," *IEEE Trans. Magn.*, Vol. 39, 3503–3506, 2003.
7. Sopanen, J., V. Ruuskanen, J. Nerg, and J. Pyrhonen, "Dynamic torque analysis of a wind turbine drive train including a direct-driven permanent-magnet generator," *IEEE Trans. Energy Convers.*, Vol. 58, 3859–3867, 2011.
8. Cistelecan, M. V., M. Popescu, and M. Popescu, "Study of the number of slots/pole combinations for low speed permanent magnet synchronous generators," *Proc. IEMDC*, 1616–1620, 2007.
9. Ge, X., G. Han, Z. Cheng, and Z. Wang, "Research of cogging torque in the brushless DC motor with fractional ratio of slots and poles," *Proc. ICEMS*, Vol. 1, 76–80, 2005.
10. Wu, D. and Z. Q. Zhu, "Design tradeoff between cogging torque and torque ripple in fractional slot surface-mounted permanent magnet machines," *IEEE Trans. Magn.*, Vol. 51, 1–4, 2015.
11. Sun, A., J. Li, R. Qu, and D. Li, "Effect of multilayer windings on rotor losses of interior permanent magnet generator with fractional-slot concentrated-windings," *IEEE Trans. Magn.*, Vol. 50, 1–4, 2014.
12. Hong, C., Q. Ronghai, L. Jian, and L. Dawei, "Demagnetization performance of a 7 MW interior permanent magnet wind generator with fractional-slot concentrated windings," *IEEE Trans. Magn.*, Vol. 51, 1–4, 2015.
13. Valavi, M., A. Nysveen, R. Nilssen, R. D. Lorenz, and T. Rolvag, "Influence of pole and slot combinations on magnetic forces and vibration in low-speed PM wind generators," *IEEE Trans. Magn.*, Vol. 50, 1–11, 2014.
14. Guemes, J. A., A. A. Iraolagoitia, J. J. Del Hoyo, P. Fernández, "Torque analysis in permanent-magnet synchronous motors: A comparative study," *IEEE Trans. Energy Convers.*, Vol. 26, 55–63, 2011.
15. Zhu, Z. Q. and D. Howe, "Influence of design parameters on cogging torque in permanent magnet machines," *IEEE Trans. Energy Convers.*, Vol. 15, 407–412, 2000.
16. Bianchi, N. and S. Bolognani, "Design techniques for reducing the cogging torque in surface-mounted PM motors," *IEEE Trans. Ind. Appl.*, Vol. 38, 1259, 2002.
17. Bianchi, N., M. Degano, and E. Fornasiero, "Sensitivity analysis of torque ripple reduction of synchronous reluctance and interior PM motors," *IEEE Trans. Ind. Appl.*, Vol. 51, 187–195, 2015.
18. Un-Jae, S., C. Yon-Do, C. Jae-Hak, H. Pil-Wan, K. Dae-hyun, and L. Ju, "A technique of torque ripple reduction in interior permanent magnet synchronous motor," *IEEE Trans. Magn.*, Vol. 47, 3240–3243, 2011.
19. Han, S.-H., T. M. Jahns, W. L. Soong, M. K. Guven, and M. S. Illindala, "Torque ripple reduction in interior permanent magnet synchronous machines using stators with odd number of slots per pole pair," *IEEE Trans. Energy Convers.*, Vol. 25, 118–127, 2010.
20. Bianchi, N., S. Bolognani, M. D. Pre, and G. Grezzani, "Design considerations for fractional-slot winding configurations of synchronous machines," *IEEE Trans. Ind. Appl.*, Vol. 42, 997–1006, 2006.
21. Grop, H., J. Soulard, and H. Persson, "Theoretical investigation of fractional conductor windings for AC-machines — definition, air-gap m.m.f. and winding factors," *Proc. ICEM*, 1–6, 2008.
22. Evans, D., Z. Azar, L. J. Wu, and Z. Q. Zhu, "Comparison of optimal design and performance of PM machines having non-overlapping windings and different rotor topologies," *IET Proc. PEMD*, 1–7, 2010.
23. Islam, M. S., R. Islam, and T. Sebastian, "Experimental verification of design techniques of permanent-magnet synchronous motors for low-torque-ripple applications," *IEEE Trans. Ind. Appl.*, Vol. 47, 88–95, 2011.
24. Zhu, Z. Q., "A simple method for measuring cogging torque in permanent magnet machines," *Proc. IEEE Conf. PES*, 1–4, 2009.
25. Islam, M. S., S. Mir, and T. Sebastian, "Issues in reducing the cogging torque of mass-produced permanent-magnet brushless DC motor," *IEEE Trans. Ind. Appl.*, Vol. 40, 813–820, 2004.
26. Heins, G., M. Thiele, and T. Brown, "Accurate torque ripple measurement for PMSM," *IEEE Trans. Instrumentation and Measurement*, Vol. 60, 3868–3874, 2011.